NASA TECHNICAL MEMORANDUM

NASA TM X- 52861

NASA TM X- 52861

SOME PERFORMANCE CHARACTERISTICS OF DIVERGENT-FIELD BOMBARDMENT THRUSTERS

by Harold R. Kaufman and Richard P. Vahrenkamp
Lewis Research Center
Cleveland, Ohio

TECHNICAL PAPER proposed for presentation at
Eighth Electric Propulsion Conference sponsored by the
American Institute of Aeronautics and Astronautics
Stanford, California, August 31 - September 2, 1970

SOME PERFORMANCE CHARACTERISTICS OF DIVERGENT-FIELD BOMBARDMENT THRUSTERS

by Harold R. Kaufman and Richard P. Vahrenkamp

Lewis Research Center
Cleveland, Ohio

TECHNICAL PAPER proposed for presentation at

Eighth Electric Propulsion Conference sponsored by the
American Institute of Aeronautics and Astronautics
Stanford, California, August 31 - September 2, 1970

NATIONAL AERONAUTICS AND SPACE ADMINISTRATION

SOME PERFORMANCE CHARACTERISTICS OF DIVERGENT-FIELD BOMBARDMENT THRUSTERS*

by Harold R. Kaufman** and Richard P. Vahrenkamp
Colorado State University
Fort Collins, Colorado

Abstract

An experimental investigation was conducted with electron-bombardment thrusters employing highly divergent magnetic fields and using mercury propellant. The performance of these thrusters was found to the first approximation to be independent of configuration changes that did not affect the primary-election region. Maximum propellant utilizations were also observed, where an increase in emission produced no increase - or even a small decrease - in beam current. The value of the maximum utilization increased with an increase in total propellant flow rate. An analysis supports the conclusion that maximum utilization corresponds to only primary electrons being in the primary-electron region of the chamber. As a final experimental observation, double-valued ion-chamber performance was obtained over a substantial range of utilization for one configuration.

Introduction

Electron-bombardment ion thrusters have been studied for about 10 years.[1, 2] During this time many investigations have been conducted to determine the effects of various configuration changes.[3-8] More recently, the performance of bombardment thrusters has been improved through the use of highly divergent magnetic-field shapes.[9, 10]

The electron population in a bombardment thruster using mercury as the propellant can be divided into two groups: primary electrons with energies corresponding to roughly the discharge potential difference, and secondary electrons that typically have a near-Maxwellian distribution centered on an energy of 3-7 ev (electron-volts).[11] The secondary electron energy is determined in a large measure by a mercury excitation level of 4.9 ev. The primary electrons have more than enough energy to reach the anode through the plasma sheath surrounding the anode. Because of this, primary electrons that reach magnetic field lines that intersect the anode tend to be collected rapidly by the anode. Thus most primary electrons are found in a "primary-electron region" defined approximately by the magnetic-field lines that do not intersect the anode. Because of the highly divergent field shapes used, the primary-electron region in most recent thruster designs is near the accelerator. By way of contrast, the primary-electron region in older thrusters occupied a much larger volume extending the length of the ion chamber.

This difference in primary-electron region is, of course, responsible for much of the improved performance of recent thruster designs. This difference is also responsible for some differences in performance characteristics, and some of these performance characteristics have not been examined thoroughly since the change to recent thruster designs. The subject of this paper, then, is some of the performance characteristics of thrusters with higly divergent field shapes, and how these characteristics differ from those of previous thruster designs.

Apparatus and Procedure

The mercury propellant thruster used in this investigation is shown in Fig. 1. The magnetic field is determined by a ring-shaped soft-iron pole piece near the accelerator and a cylindrical soft-iron pole piece near the cathode. These pole pieces are connected by four soft-iron paths (each about 3.2 mm by 12.7 mm, in cross section) on which the field windings are mounted. The cylindrical pole piece has about the same cross section as the total of the four paths, and also has a field winding for most of its length. The construction of the four soft-iron paths permitted axial motion of the cylindrical pole piece for initial optimization. Thereafter, the cylindrical pole piece was held fixed. The data presented in this paper were obtained with the central pole piece 3.5 cm from the accelerator, a location that gave good performance over a wide range of utilization. Experimental data were taken at various magnetic-field currents, but the data presented are limited to a current of 2 amps. The field on the axis of the thruster, and between the central pole piece and the screen grid, is indicated in Fig. 2 for this 2-amp field current.

A 71 percent open area screen was used to reduce ion recombination on the screen. Only holes completely within a 10-cm diameter circle were used to accelerate ions, and there were 429 such holes in the accelerator design used. A screen-accelerator spacing of 2-2.5 mm was used, and the positive and negative potentials used for the data herein were +3 kv and -1.5 kv.

The thruster was operated in the 1.2-m diameter, 4.8-m long Space Propulsion Research Facility located in the Engineering Research Center of Colorado State University. The normal pressure obtained in this facility with the thruster operating was $3\text{-}4\times10^{-6}$ torr.

Effect of Ion-Chamber Configurations

Early bombardment-thruster designs typically had an extensive volume occupied by primary electrons, as indicated in Fig. 3. Because the region occupied by primary electrons in this design extends the full length of the ion chamber, a change in ion-chamber length will clearly affect the primary electrons. The primary-

*This research supported in part by Colorado State University.
**On graduate-study leave from NASA Lewis Research Center, Cleveland, Ohio.

electron region indicated in Fig. 3 is, of course, somewhat idealized. The finite cyclotron radius of primary electrons leads to a boundary with finite thickness instead of the line thickness of a limiting magnetic field line - as indicated in Fig. 3. With recent divergent-field designs, however, the primary-electron region is localized near the screen. For the thruster under investigation in this paper, the primary-electron region is indicated in Fig. 4. As shown in Fig. 4, the primary-electron region is independent of chamber geometry unless the chamber is made very short.

The performance of several ion-chamber configurations that have the same shape of primary electron region - as well as field strength - is indicated in Fig. 5. To reduce the data spread due to different propellant flow rates, the performance shown in Fig. 5 is also limited to a narrow range from 135 to 151 ma equivalent (the current that would result if each propellant atom carried one electronic charge). The major conclusion to be drawn from Fig. 5 is that the performance is roughly the same (±15 percent) for a wide range of ion-chamber configurations. It appears reasonable to conclude that this similarity is due to the similarity in primary-electron regions. A thorough study of ion-chamber processes[11] has shown that about half of the ions are produced by collisions of primary electrons with neutrals, and about half from the Maxwellian "tail" of the secondary electrons. While the primary electrons produce ions near the screen grid in a divergent-field design, the secondary electrons produce ions throughout the chamber. The ions from primary electrons are thus far more likely to be extracted and accelerated into the beam. To a first approximation, then, the performance of a divergent-field thruster might be expected to be determined by the primary electrons.

Recent studies[11, 12] have noted that the ion-chamber losses are greater than the theoretical value of 60-80 ev/ion by roughly the ratio of total ion-chamber wall area to beam area. The possibility of using the total-to-beam area ratio as a simple engineering design tool is appealing, but suffers from a serious shortcoming. This shortcoming can be shown by crossplotting the data of Fig. 5 at 50 percent propellant utilization. (Performance at high utilizations will be considered in following sections of this paper.) As shown in the crossplot of Fig. 6, the total-to-beam area ratio changes by a factor of 4 with only about a 25 percent change in losses. Thus the increase of losses with wall area is considerably less than a proportional increase. While the performance of many recent divergent-field thrusters would appear to support the use of a total-to-beam area ratio as a design tool, the data of Fig. 6 clearly show that large increases in wall area can be used with only small increases in losses. Such a design tool would thus have little generality.

Maximum Propellant Utilization

A number of cases were observed during the operation of the thruster where a further increase in cathode emission was accompanied by no increase - or even a small decrease - in beam current, as shown for discharge (anode) currents above 1 amp in Fig. 7. (This condition should not be confused with the space-charge limitation for the cathode. In this latter condition an increase in cathode-heater power also results in no significant increase in beam current, but the cathode emission is essentially a constant despite the heater-power increase.) The maximum utilizations that were obtained in the manner indicated by Fig. 7 are plotted against total propellant flow rate in Fig. 8(a). A clear general trend of increasing maximum utilization with increasing neutral flow is shown. When plotted in terms of the un-ionized propellant leaving the thruster (Fig. 8(b)), these same data gave approximately a constant value despite the range in total propellant flow. To make sure that the ordinate of Fig. 8(b) is understood, it is defined by

$$J_{o\,|\,\text{un-ionized}} = \left(1 - \eta_{u,\,\max}\right) J_{o\,|\,\text{total}} \qquad (1)$$

The points that depart the most from the general pattern in Fig. 8 were obtained with the large diameter chamber. The most likely explanation of this departure involves the short cylindrical section of 10-cm anode used in the large diameter configuration (see Fig. 1). All the primary electrons that reach the anode do not impinge on the downstream edge, as might be implied by the idealization of Fig. 3. Instead, one would expect an extended current distribution, with the extent proportional to the primary-electron cyclotron radius. To be similar (for the primary-electron region) to the small diameter configurations, then, the short cylindrical section should still be long compared with the cyclotron radius of the primary electrons. This cylindrical section was 0.6 cm long, while a 30-ev electron has a cyclotron radius of over 1 cm in this region. The desired condition for similarity was therefore not met. A difference within about 1 cm of the short cylindrical anode section affects only a small fraction of the volume occupied by the primary eletron region, and thus should not have affected the performance at low utilizations. A large fraction of the ion-chamber cross section is affected, though, so that maximum utilization might well have been adversely affected. Data from the large diameter configuration will therefore be omitted from subsequent maximum-utilization considerations.

Analysis of Maximum-Utilization Data

The trends of Figs. 8(a) and 8(b) can be reproduced analytically by assuming that only primary electrons are in the primary-electron region. That is, the maximum utilization is assumed to be reached when the addition of primary electrons is so rapid that the density of primary electrons is sufficient to neutralize the ions that are present. Thus the Maxwellian electrons that would otherwise be present are not required to neutralize the ions.

Consider first the total ion production $\dot{N}$ from primary electrons. Using mean values for the primary-electron region,

$$\dot{N} = n_e\, v_e\, n_o\, \sigma V_p \qquad (2)$$

where n_e and v_e are the primary electron density and velocity, n_o and σ are the neutral density and ionization cross section, and V_p is the volume of the primary-

electron region. For the total loss rate of ions from this region,

$$\dot{N} = n_i v_i A_p \tag{3}$$

where n_i and v_i are the ion density and velocity towards the outer boundary of the primary-electron region, and A_p is the area of this outer boundary. The ion velocity towards the outer boundary can be estimated from the Bohm criteria for a stable sheath.[13]

$$v_i = \sqrt{\frac{kT_e}{m_i}} \tag{4}$$

This relationship assumes a Maxwellian electron distribution, but should be approximately valid for a non-Maxwellian distribution of primary electrons alone as long as T_e corresponds to the mean energy for the primary electrons. For primary electrons alone, the Bohm criteria can be approximated as

$$v_i = v_e \sqrt{\frac{m_e}{2m_i}} \tag{5}$$

The primary-electron region is many Debye shielding lengths in extent, so that the net charge must be essentially zero. Thus we can equate

$$n_e = n_i \tag{6}$$

With the substitution of Eqs. (5) and (6) into (3), and the equating of ion loss and production rates (Eqs. (2) and (3)), one finds

$$n_o = \sqrt{m_e/2m_i}/\sigma(V_p/A_p) \tag{7}$$

With mercury used for m_i and 5×10^{-20} m^2 used for σ, this becomes (mks system)

$$n_o = 2.34\times10^{16}/(V_p/A_p) \tag{8}$$

This equation can be particularized for the thruster investigated herein. The value for V_p/A_p was determined from Fig. 4 as about 0.011 m. With this substitution

$$n_o = 2.1\times10^{18}/m^3 \tag{9}$$

This neutral density can be expressed as a neutral loss rate. The total restriction of the accelerator system was estimated as equivalent to a sharp-edged orifice whose area is 40 percent of the total 10-cm beam area. The neutral temperature was estimated at 500 K. With these assumptions, one can find the equivalent current for lost neutrals from Eq. (9)

$$J_o \,|\, \text{un-ionized} = 0.037 \text{ amp} \tag{10}$$

Eq. (10) was used for the theoretical curve in Fig. 8(b). The maximum utilization can be obtained in turn from Eq. (10) as

$$\eta_{u,\,max} = (J_o \,|\, \text{total} - 0.037)/J_o \,|\, \text{total} \tag{11}$$

Eq. (11) was used for the theoretical curve in Fig. 8(a).

The theoretical values of maximum utilization and un-ionized propellant appear to agree closely with the experimental data in Figs. 8(a) and (b). The agreement, however, is not as good as it appears-as can be shown by considering points at higher total propellant flow rates. Although maximum utilizations were not obtained for these higher flow rates, lower bounds for these maximum utilizations were obtained. (The lower bound for maximum utilization is simply the highest value that was obtained, without actually obtaining data of the form shown in Fig. 7.) The data of Fig. 8 are replotted with these additional lower limits in Fig. 9. The preceding theoretical treatment (solid line in Fig. 9) clearly shows too low a maximum utilization at higher values of total propellant flow rate.

Because of the escape of neutrals through the accelerator system, the neutral density should be low at this boundary of the primary-electron region. The mean value of neutral density that should be used in Eq. (7) might therefore be expected to correspond to a value higher than $J_o \,|\, \text{un-ionized}$. If a mean value of

$$J_o \,|\, \text{mean} = \sqrt{(J_o \,|\, \text{total})(J_o \,|\, \text{un-ionized})} \tag{12}$$

is used instead of $J_o \,|\, \text{un-ionized}$, a theoretical prediction following the dotted lines of Fig. 9 is obtained. As is evident from Fig. 9, this new prediction may overestimate the variation with total propellant flow rate.

In summary, there is uncertainty as to the proper definition of neutral density to use in the maximum utilization prediction or even whether the same definition will work for all thruster configurations. From the qualitative agreement between the data and prediction - both in level and variation with flow rate - the broad features of the proposed explanation for a maximum utilization appear justified. Hopefully, the quantitative problems will be resolved if more complete utilization data are obtained.

Double-Valued Performance

Fig. 7 shows double values for ion-chamber performance over a small range of propellant utilization. One might therefore wonder if double values are possible at other values of propellant utilization. The answer - at least in part - is yes, as indicated in Fig. 10. The significance of the data presented in Fig. 10 was not immediately recognized at the time the data were obtained, hence very little of this type of data was recorded. It was noted, though, that several configurations exhibited double-valued performance of roughly the same type. The SERT II development program can also be cited as further evidence that the double-valued performance shown is more than an isolated problem. During

this program a "low-mode" operation was encountered where discharge parameters were near normal, but the beam current was only a fraction of normal. As often happens in a development program, though, time was available to find ways to avoid the problem, but not to understand it. Other investigations[14, 15] have also indicated the possibility of similar double-valued performance, but ion-chamber data of the type shown in Fig. 10 were not included. (With cesium propellant, the equilibration of emitted electrons is so rapid that the electrons form one near-Maxwellian distribution. Double-valued operation with cesium,[14] therefore, may - or may not - be similar to double-valued operation with mercury.)

The data of Fig. 10 show a hysteresis loop. The data of this loop were obtained by varying emission at roughly constant discharge voltage (hand regulated). Two isolated points are also shown that appear to extend the upper curve to low utilizations. However, both of these points were obtained by starting from low utilizations. The lower of the two points required a higher discharge voltage (32.5 V) than the usual 30 V. The drop back to the lower curve in the hysteresis loop of Fig. 10, then, might have been due to operation not being possible at 30 V with further reductions in discharge current. Operation at a higher discharge voltage might, in this case, have avoided this drop to the lower (more efficient) curve. The cause of this double-valued operation is not clear at the present time. From the analysis of maximum utilization, one might suspect that the performance of the upper curve corresponds to substantially higher electron energies. More detailed data, though, will probably be required to make an explanation that is more than speculation.

Concluding Remarks

Several performance characteristics of divergent-field thrusters have been presented herein. The first is the insensitivity to configuration changes that do not affect the primary electron region. Or, conversely, the major performance characteristics should be determined by the spatial distribution of primary electrons. This does not mean that only the primary electron region has any significance. The ±15 percent variation due to changes outside of the primary electron region may still be involved in reaching required performance objectives, and hence be the subject of extensive investigations.

The implied assumption in most previous ion chamber studies has been a gradual asymptotic approach to 100 percent utilization with increased emission. The reduced volume of the primary-electron region has apparently made the phenomenon of maximum utilization easier to reach, and thus observe, in designs employing highly divergent magnetic fields. The explanation of this limit as corresponding to all the plasma electrons being primary electrons (in the primary-electron region) is given good qualitative support by the analysis presented herein. Further investigation appears necessary to put this analysis on a firm quantitative footing.

Double-valued ion chamber operation for a single utilization has also been observed. At present there is little understanding of the cause for this double-valued performance.

References

1. Kaufman, H. R., "An Ion Rocket with an Electron-Bombardment Ion Source," TN D-585, 1961, NASA, Cleveland, Ohio.

2. Kaufman, H. R. and Reader, P. D., "Experimental Performance of Ion Rockets Employing Electron-Bombardment Ion Sources," Progress in Astronautics and Rocketry, Vol. 5 - Electrostatic Propulsion, D. B. Langmuir, E. Stuhlinger, and J. M. Sellen, Jr., eds., Academic Press, New York, 1961, pp. 3-20.

3. Reader, P. D., "Investigation of a 10-Centimeter-Diameter Electron-Bombardment Ion Rocket," TN D-1163, 1962, NASA, Cleveland, Ohio.

4. Kerslake, W. R., "Accelerator Grid Tests on an Electron-Bombardment Ion Rocket," TN D-1168, 1962, NASA, Cleveland, Ohio.

5. Reader, P. D., "Scale Effects on Ion Rocket Performance," ARS Journal, Vol. 32, No. 5, May 1962, pp. 711-714.

6. Speiser, R. C., Kilpatrick, W. D., and Reid, G. C., "Study of a Gas Discharge Cesium Ion Source," EOS-2120-Final, NASA CR-52366, July 26, 1963, Electro-Optical Systems, Inc., Pasadena, Calif.

7. Reader, P. D., "Experimental Effects of Propellant-Introduction Mode on Electron-Bombardment Ion Rocket Performance," TN D-2587, 1965, NASA, Cleveland, Ohio.

8. Sohl, G., Fosnight, V. V., Goldner, S. J., and Speiser, R. C., "Cesium Electron-Bombardment Ion Microthrusters," Journal of Spacecraft and Rockets, Vol. 4, No. 9, Sept. 1967, pp. 1180-1183.

9. Bechtel, R. T., "Discharge Chamber Optimization of the SERT II Thruster," Paper 67-668, Sept. 1967, AIAA, New York, N.Y.

10. Kerrisk, D. J. and Kaufman, H. R., "Electric Propulsion Systems for Primary Spacecraft Propulsion," Paper 67-424, July 1967, AIAA, New York, N.Y.

11. Masek, T. D., "Plasma Properties and Performance of Mercury Ion Thrusters," Paper 69-256, Mar. 1969, AIAA, New York, N.Y.

12. Milder, N. L., "A Survey and Evaluation of Research on the Discharge Chamber of a Kaufman Thruster," Paper 69-494, June 1969, AIAA, New York, N.Y.

13. Bohm, D., "Minimum Ionic Kinetic Energy for a Stable Sheath," The Characteristics of Electrical Discharges in Magnetic Fields, A. Guthrie and R. K. Wakerling, eds., McGraw-Hill, New York, 1949, pp. 77-86.

14. Worlock, R. M., Sohl, G., Trump, G., et al., "Cesium Bombardment Ion Engine System Development," EOS-7146-F, AFAPL-TR-69-87, Oct. 1969, Electro-Optical Systems, Inc., Pasadena, Calif.

15. Pawlik, E. V., Costogue, E. N., and Schaefer, W. C., "Operation of a Lightweight Power Conditioner with a Hollow Cathode Ion Thruster," Paper 70-648, June 1970, AIAA, New York, N. Y.

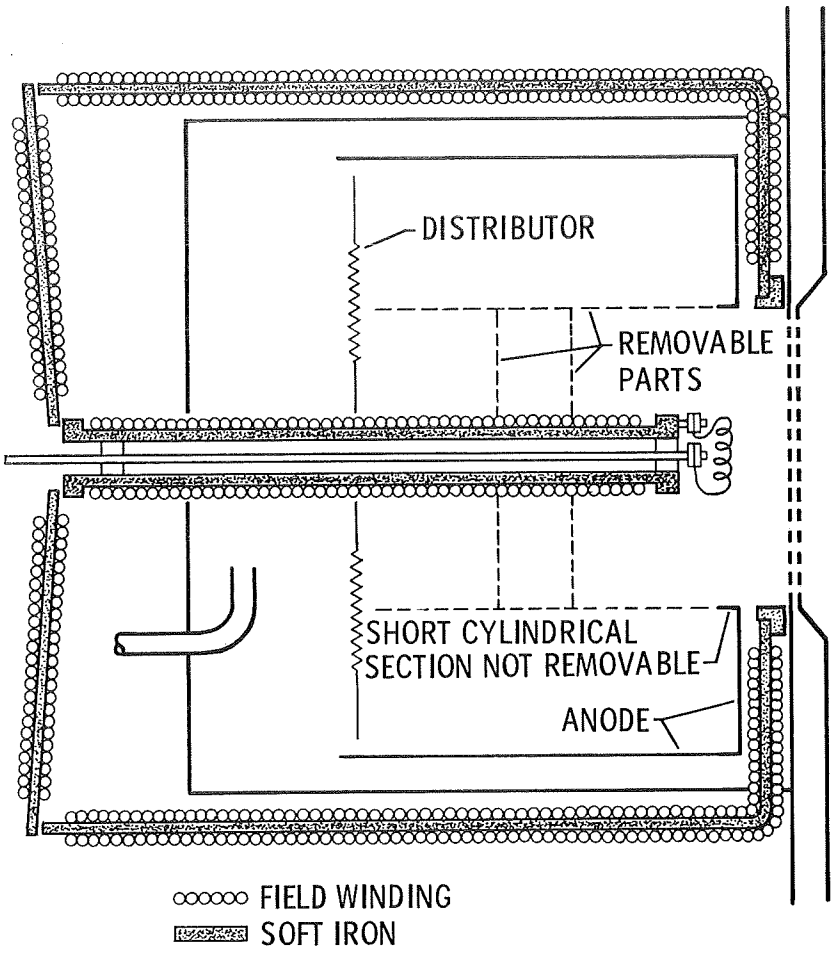

Figure 1. - Thruster with adjustable ion chamber.

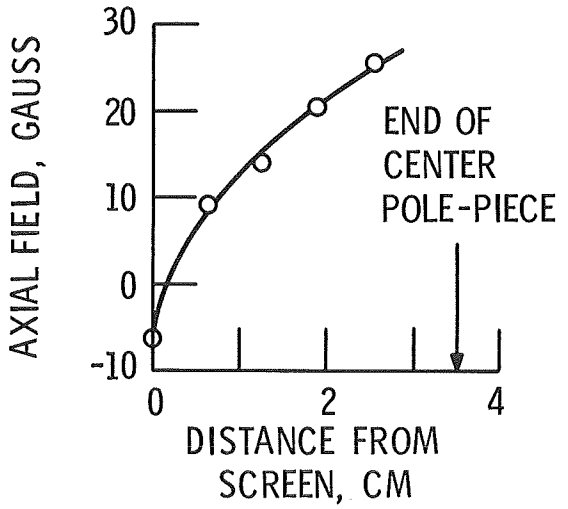

Figure 2. - Field on axis of thruster with 2-ampere field-winding current.

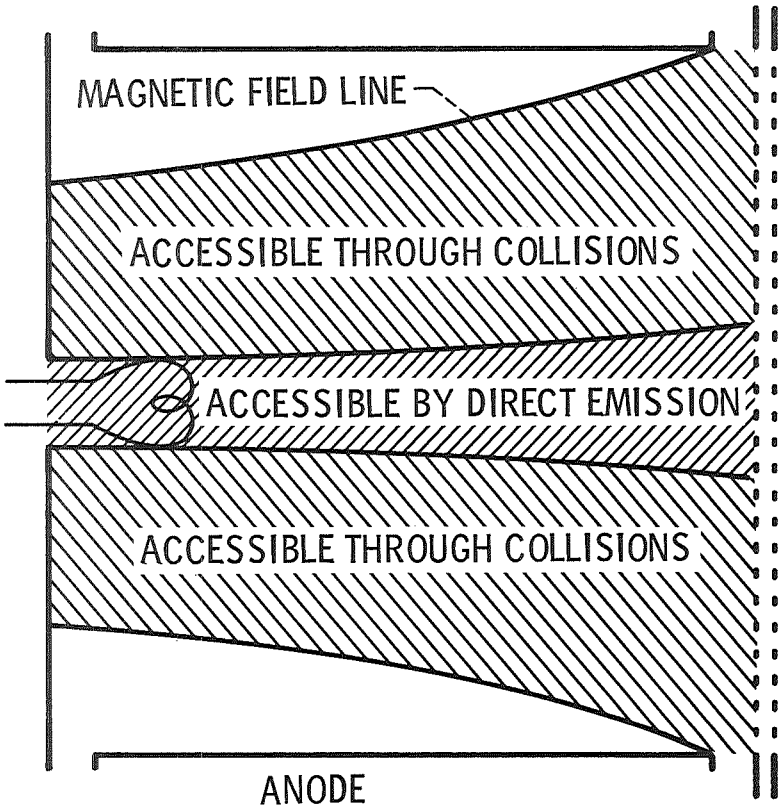

Figure 3. - Primary-electron region (shown by crosshatching) in early bombardment thruster design.

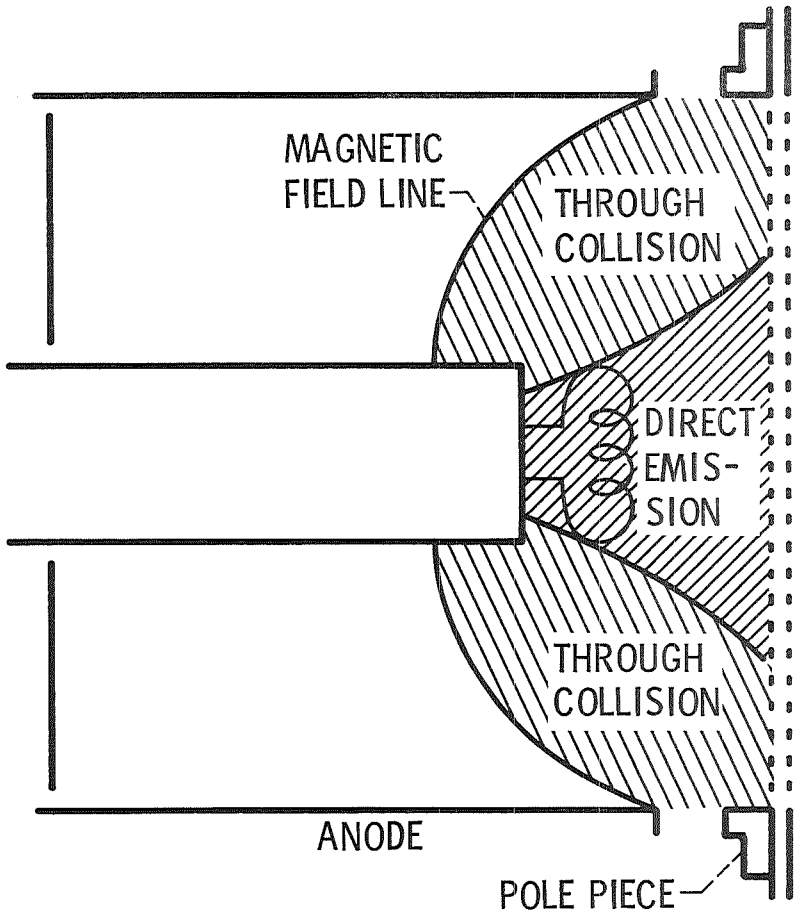

Figure 4. - Primary-electron region (shown by crosshatching) in divergent field thruster used in this investigation.

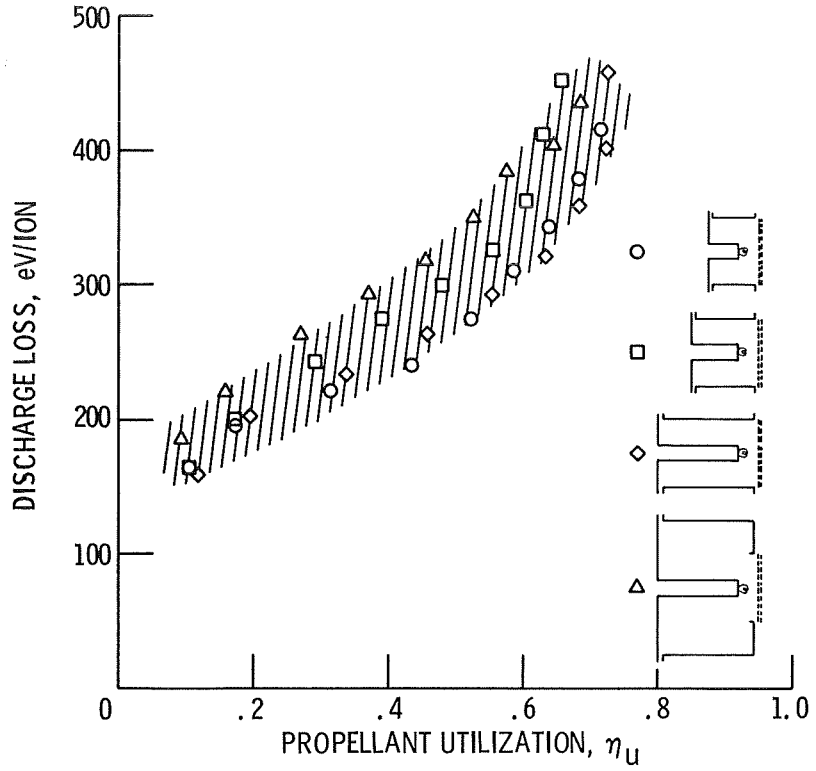

Figure 5. - Performance of several ion-chamber configurations with similar primary-electron regions. Propellant mass flow ranged from 135 to 151 mA equivalent (1.01 to 1.13 gm/hr).

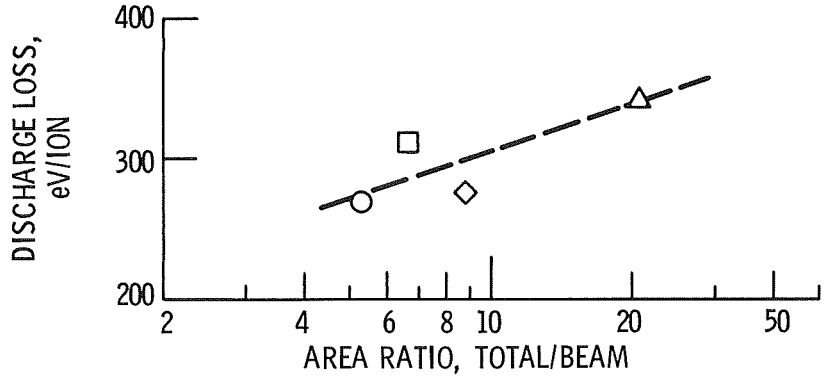

Figure 6. - Variation of discharge loss with ion-chamber area ratio. The area ratio is defined as total surface area of ion chamber divided by the beam area. This is a cross-plot of figure 5 at 50 percent utilization. (See fig. 5 for symbol definitions.)

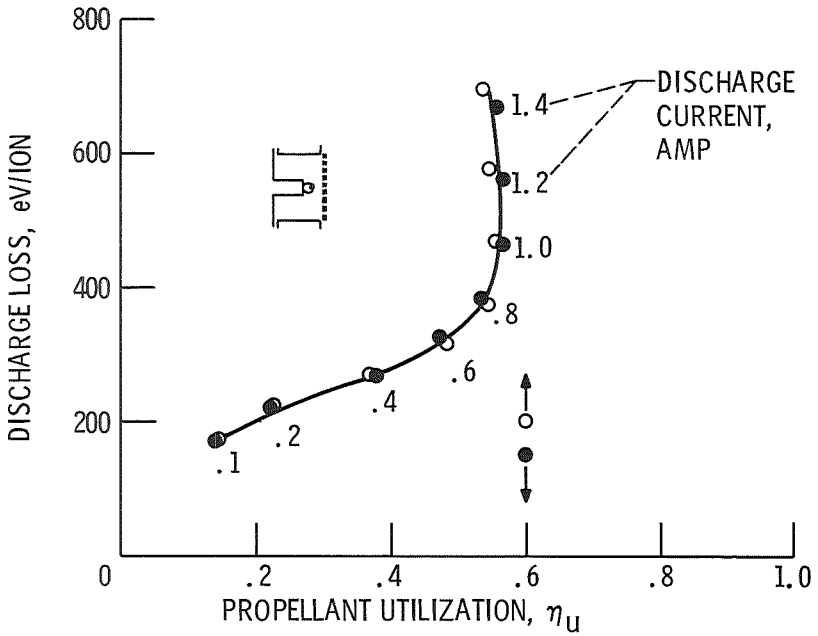

Figure 7. - Ion-chamber performance showing maximum propellant utilization. Propellant mass flow, 108 mA equivalent (0.81 gm/hr).

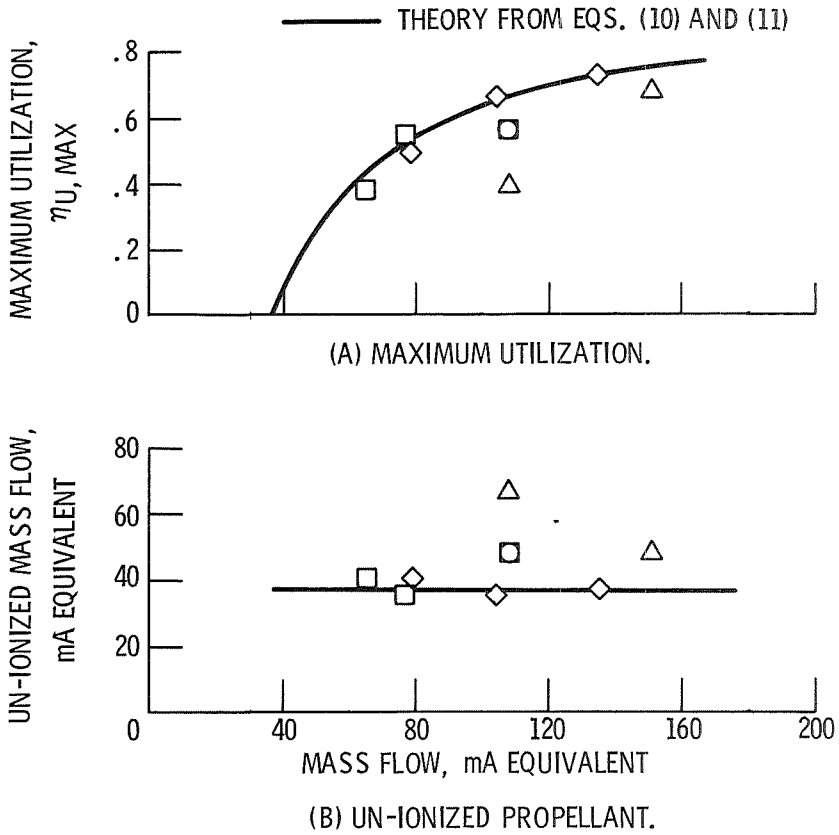

Figure 8. - Effect of propellant mass flow at maximum utilization. (See fig. 5 for symbol definitions.)

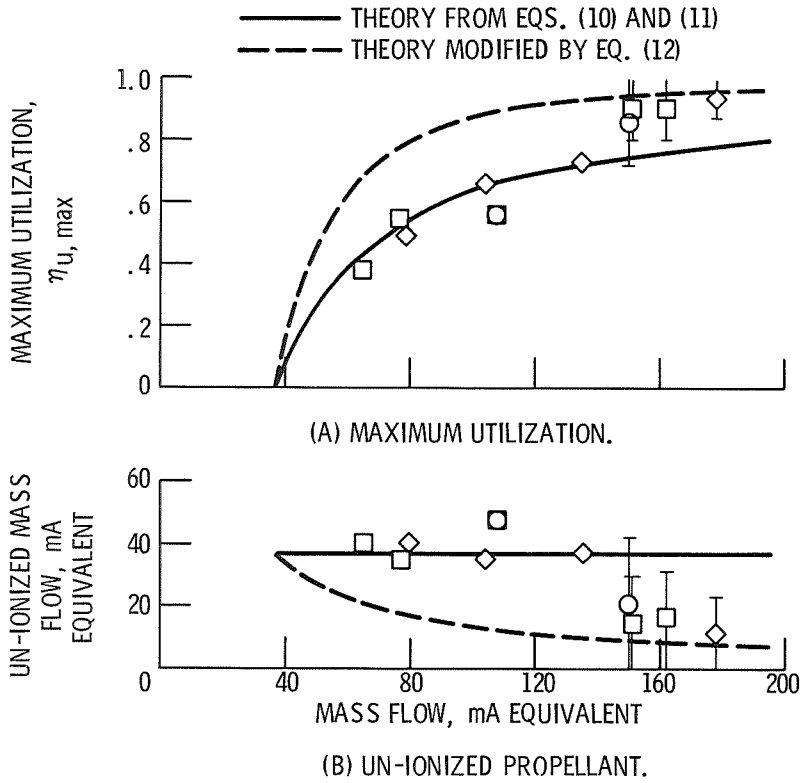

Figure 9. - Effect of propellant mass flow at maximum utilization. (See fig. 5 for symbol definitions.)

NASA-Lewis

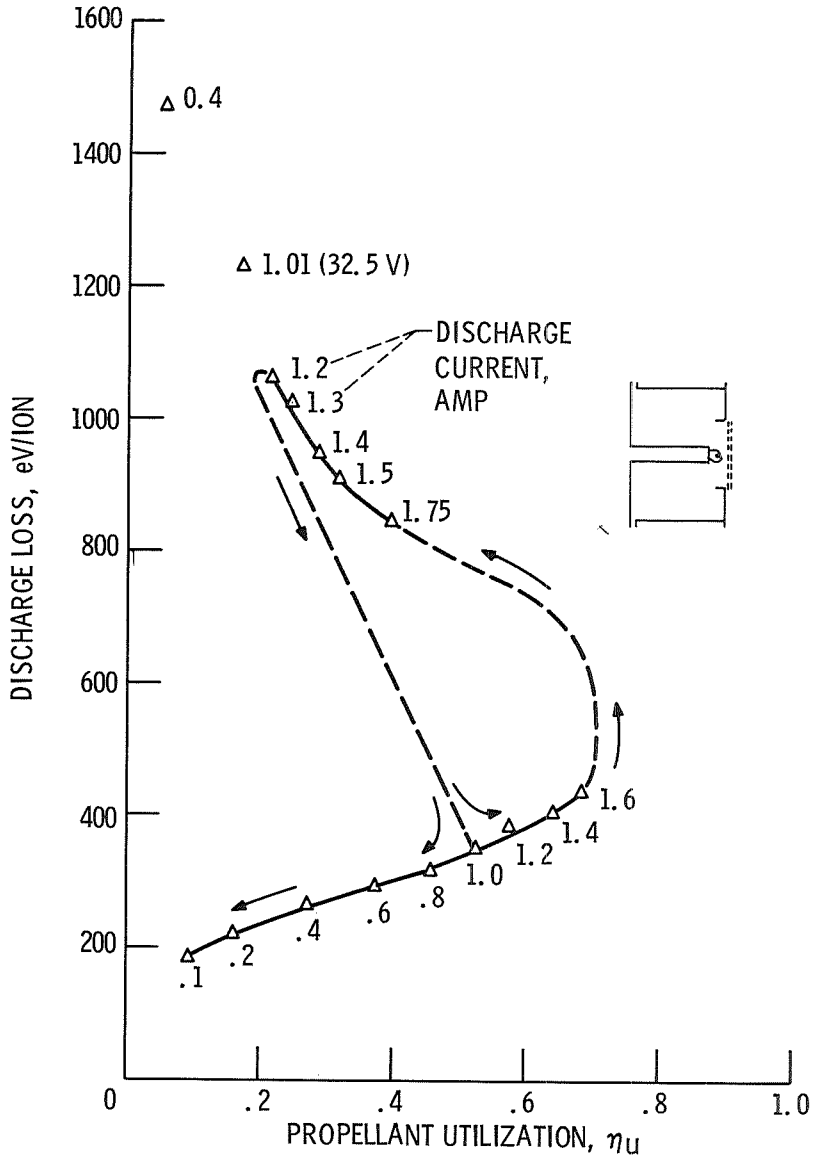

Figure 10. - Ion-chamber performance showing double-valved operation. Propellant mass flow, 151 mA equivalent (1.13 gm/hr).